Supporting Information:

Superior energy storage performance in $(Bi_{0.5}Na_{0.5})TiO_3$-based lead-free relaxor ferroelectrics for dielectric capacitor application via multiscale optimization design

Chongyang Li,[a] Jikang Liu,[a] Wangfeng Bai, [a*] Shiting Wu, [a] Peng Zheng,[a*] Jingji Zhang,[b] Zhongbin Pan,[c] Jiwei Zhai[d*]

[a] College of Materials and Environmental Engineering, Hangzhou Dianzi University, No. 2 Street, Hangzhou, China E-mail: bwfcxj@126.com (Wangfeng Bai), zhengpeng@hdu.edu.cn (Peng Zheng)

[b] College of Materials Science and Engineering, China Jiliang University, Hangzhou, 310018, China

[c] School of Materials Science and Chemical Engineering, School of Physical Science and Technology, Ningbo University, Ningbo, Zhejiang, 315211, China

[d] Functional Materials Research Laboratory, School of Materials Science Engineering, Tongji University, No. 4800 Caoan Highway, Shanghai, China E-mail: apzhai@tongji.edu.cn (Jiwei Zhai)

Experimental section

Sample preparation: The ceramics of (1-x)[0.955($Bi_{0.5}Na_{0.5}$)TiO_3-0.045Ba($Al_{0.5}Ta_{0.5}$)O_3]-x$CaTiO_3$ (abbreviated as BNT-BAT-*x*CT, x=0.1, 0.2, 0.3, 0.4) were synthesized by a conventional solid-state reaction method. The raw powders including Bi_2O_3, Na_2CO_3, TiO_2, $BaCO_3$, Al_2O_3, Ta_2O_5, $CaCO_3$ (≥99%) were weighed as the stoichiometric ratio for 0.955($Bi_{0.5}Na_{0.5}$)TiO_3-0.045Ba($Al_{0.5}Ta_{0.5}$)O_3 (BNT-BAT) and $CaTiO_3$ (CT). The weighed powders were ball milled in anhydrous ethanol under 330 rpm for 24h. The BNT-BAT powders were calcined at 850℃ for 6h and the CT powders were calcined at 1000℃ for 3h in air atmosphere. Two kinds of powders were remixed and then ball-milled again for 24 hours. After dried, the mixture with 8 wt% PVA was pressed into pellets with 1mm thickness and a diameter of 10mm. After removing the organic binder at 550℃ for 10h, the pressed disks were sintered at 1140-1180°C for 2h to obtain ceramic samples. Finally, the sintered ceramics were grinded and polished to 80-100 μm in thickness and then sputtered with gold electrodes (~0.00785 cm^2 and 1 mm in diameter) for ESP measurements

Sample characterization: The phase structures of samples at room temperature were identified by X-ray diffractometer (XRD; MiniFlex600, Rigaku, Japan). The surface microstructure and elements distribution of the sintered ceramics were characterized by the field emission scanning electron microscope (FE-SEM, S-4200, Hitachi, Tokyo, Japan). The Raman spectrum was provided by Raman scattering spectrometer (Horiba/Jobin Yvon, Villeneuve d'Ascq, France). Piezoresponse force microscopy (PFM) measurements were carried out using atomic force microscopy (AsylumResearch MFP-3D). For PFM measurement, the samples are polished and the surface roughness mauntains a relatively low level less than 10nm, and the ac voltage amplitude and frequency for visualizing the domain structures are 2.5V and 380kHz. The TEM sample was carefully prepared by ion milling system (Gatan 695, USA). The domain morphology observation and high-resolution atomic imaging were performed on a field-emission TEM (FEI Talos F200X, USA) at the accelerating voltage of 200 kV. The dielectric properties were measured using a High-precision LCR meter (HP

4990 A; Agilent, Palo Alto, CA). The polarization electric field (*P*-*E*) hysteresis loops, current-electric field (*I*-*E*) curves, and FORC loops were analyzed by a ferroelectric measuring system (RT1-Premier II, Radiant Technologies InC, USA). An ultraviolet spectrophotometer (TU-1901, Beijing Purkinje General Instrument, China) was applied to obtain the values of E_g. A commercial charge-discharge platform (CFD-003, Gogo Instruments Technology, China) was employed to characterize the charge-discharge performance.

Phase-field breakdown model: To explore the mechanism for the enhanced breakdown strength caused by the difference in grain size, a scalar spatially and temporally dependent damage field s (x, t) is adopted to probe the breakdown process of the BNT-BAT-xCT ceramics with different grain sizes [1-4]. The value of s varies from 1 to 0, representing the intact state and the fully damaged state, respectively. The theoretical model in this work is built through the following mathematical expressions into COMSOL Multiphysics [5, 6]:

$$\begin{cases} \bar{\nabla}\cdot\left[\varepsilon_g(s)(1+\bar{k}\bar{\nabla}\bar{\emptyset}\cdot\bar{\nabla}\bar{\emptyset})^{-\frac{1}{3}\bar{\nabla}\bar{\emptyset}}\right]=0 \\ \dfrac{\partial_s}{\partial_t}=-\dfrac{3\varepsilon_g^{'}(s)}{4\bar{k}}\left[(1+\bar{k}\bar{\nabla}\bar{\emptyset}\cdot\bar{\nabla}\bar{\emptyset})^{\frac{2}{3}}-1\right]+f^{'}(s)+\dfrac{1}{2}\bar{\nabla}^2 s \end{cases} \#(1)$$

$$\begin{cases} \bar{\nabla}\cdot\left[\varepsilon_{gb}^{'}(s)\bar{\nabla}\bar{\emptyset}\right]=0 \\ \dfrac{\partial_s}{\partial_t}=-\dfrac{\varepsilon_{gb}^{'}(s)}{2}\bar{\nabla}\bar{\emptyset}\cdot\bar{\nabla}\bar{\emptyset}+f^{'}(s)+\dfrac{1}{2}\bar{\nabla}^2 s \end{cases} \#(2)$$

The FORC distribution：In this work, E_{max} is set to be 120 kV/cm, Δα= Δβ= ΔE= 4.8 kV/cm. An approximate method to calculate $p(\alpha,\beta)$ is

$$p(\alpha,\beta)=\frac{1}{2}\frac{\partial P^2(\alpha,\beta)}{\partial\alpha\partial\beta}$$

where $p(\alpha,\beta)$ is the polarization of the FORC loop, α is the reversal electric field, β is the real electric field [7-10].

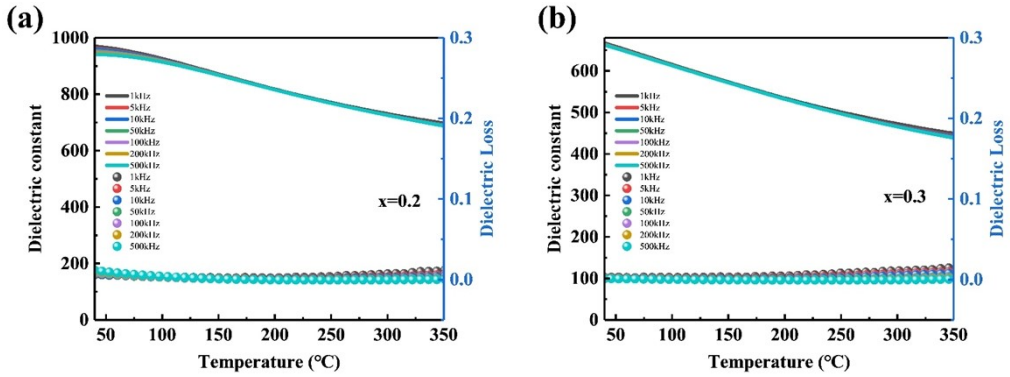

Fig. S1. Temperature-dependent dielectric constant and loss of BNT-BAT-xCT ceramics measured at different frequency: (a) x=0.2, (b) x=0.3.

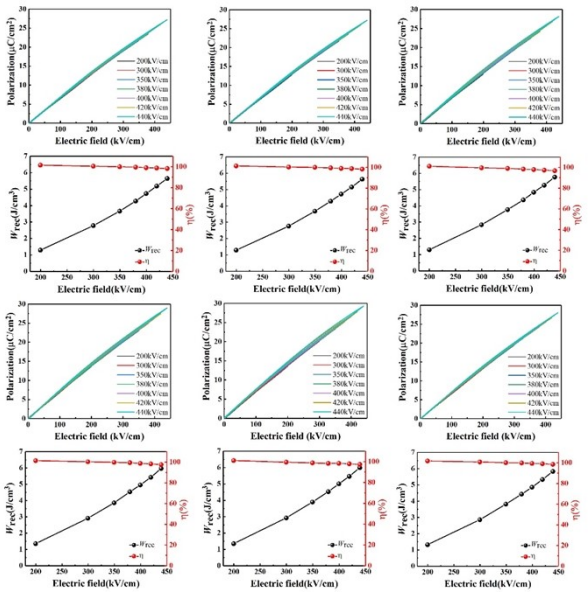

Fig. S2. Six unipolar *P-E* loops and the corresponding variation of W_{rec} and η with the electric field for x=0.4 ceramic.

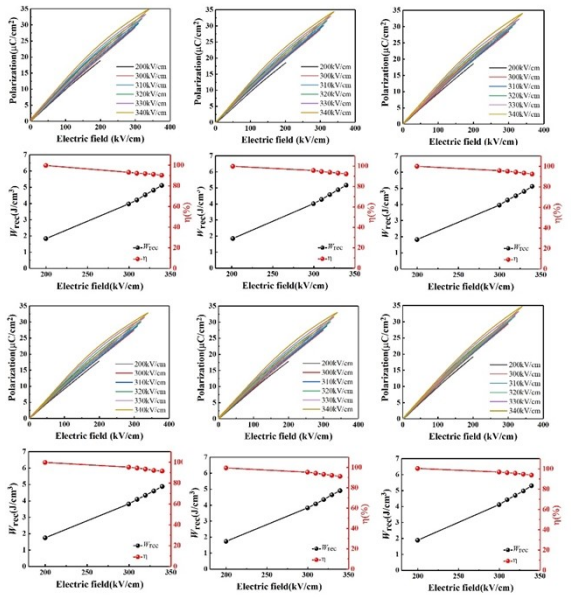

Fig. S3. Six unipolar *P-E* loops and the corresponding variation of W_{rec} and η with the electric field for x=0.3 ceramic.

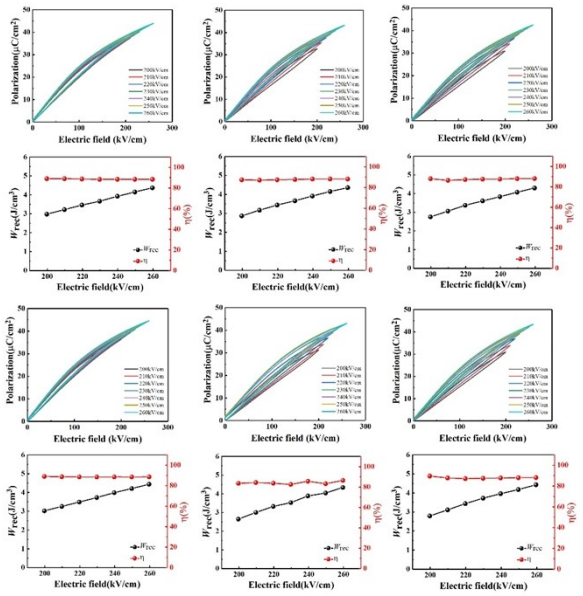

Fig. S4. Six unipolar *P-E* loops and the corresponding variation of W_{rec} and η with the electric field for x=0.2 ceramic.

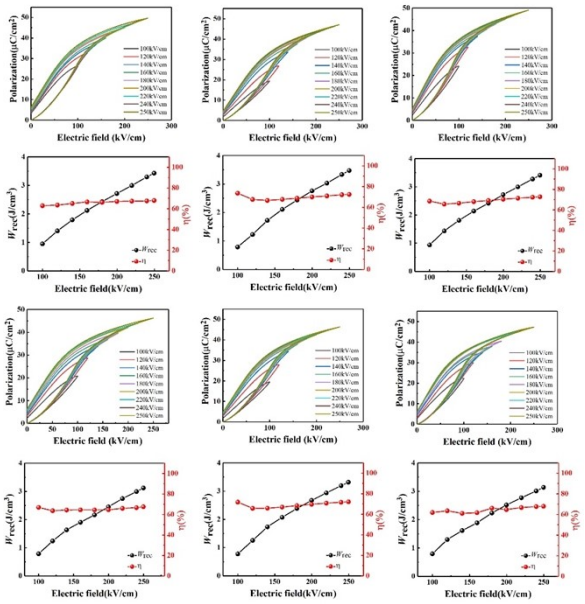

Fig. S5. Six unipolar *P-E* loops and the corresponding variation of W_{rec} and η with the electric field for x=0.1 ceramic.

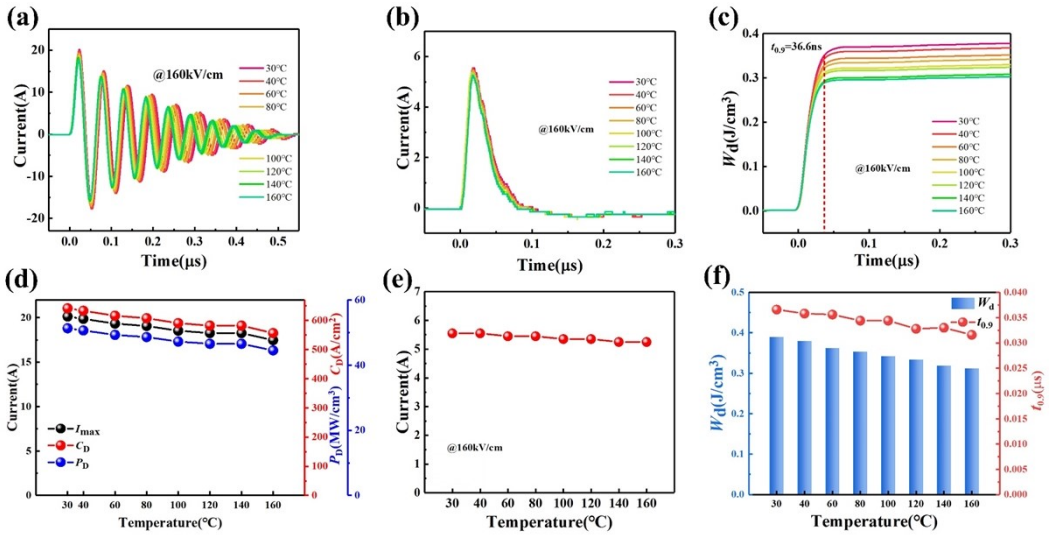

Fig. S6. Temperature-dependent (a) underdamped discharge curves, (b) overdamped discharge curves, (c) W_d-t curves, (d) the variations of I_{max}, C_D and P_D, (e) the variation of I_{max}, and (f) the changes of W_d and $t_{0.9}$ for x=0.4 ceramic.

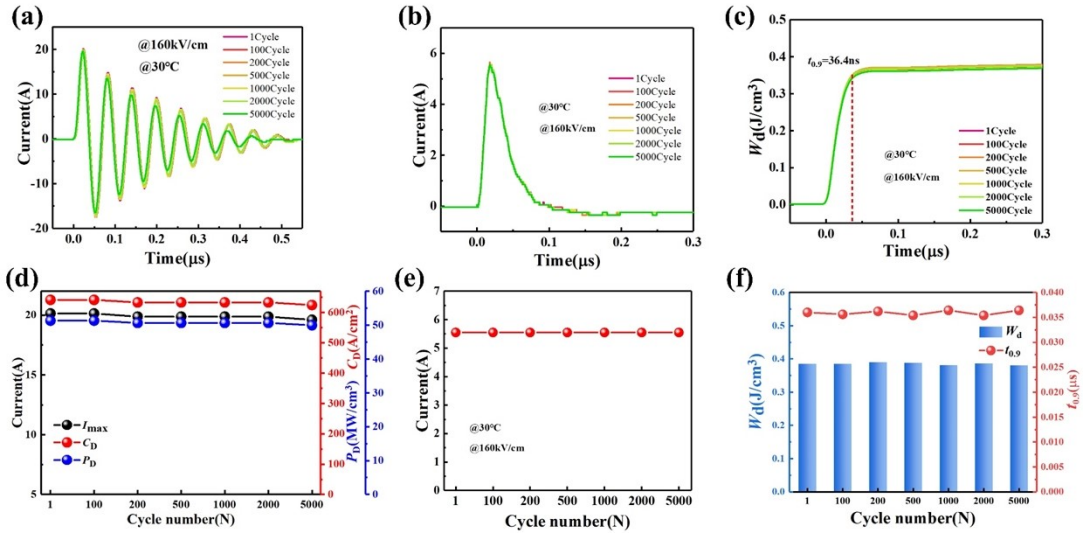

Fig. S7. Cycle number-dependent (a) underdamped discharge curves, (b) overdamped discharge curves, (c) W_d-t curves, (d) the variations of I_{max}, C_D and P_D, (e) the variation of I_{max}, and (f) the changes of W_d and $t_{0.9}$ for x=0.4 ceramic.

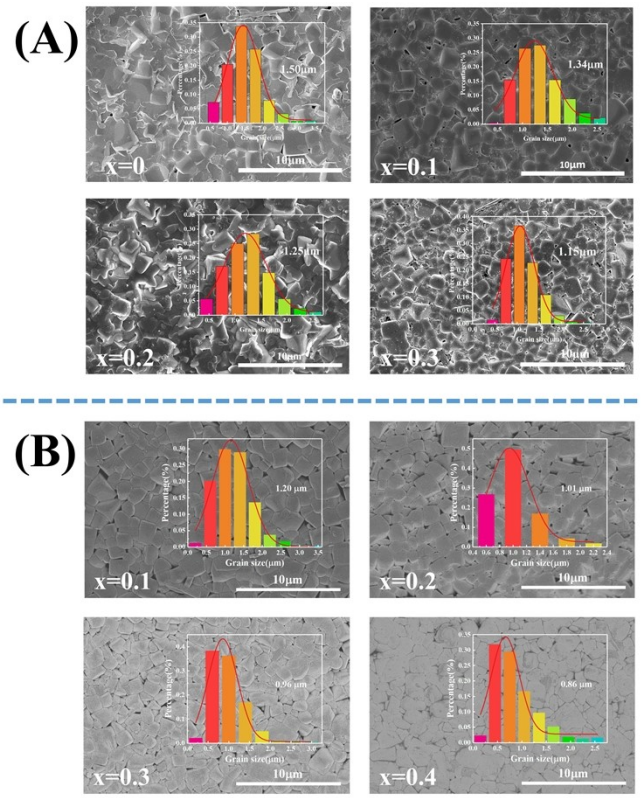

Fig. S8. The morphology and corresponding grain size distribution of the as-sintered surface (A) and the polished and thermally etched cross-sections (B) for BNT-BAT-xCT ceramics.

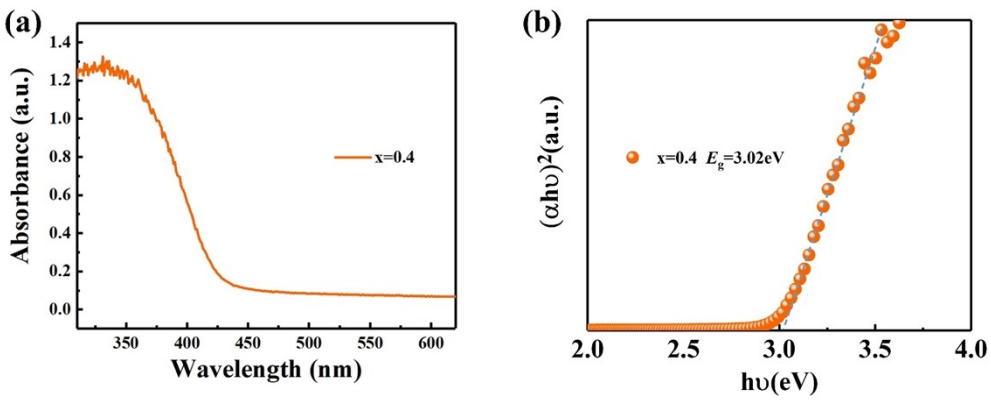

Fig. S9. (a) UV-Vis absorbance spectra and (b) $(\alpha h\nu)^2$ versus hν plot of BNT-BAT-0.4CT ceramic.

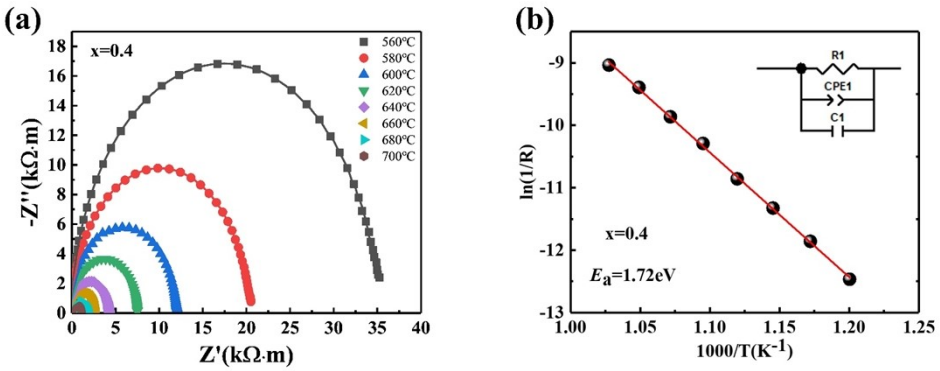

Fig. S10. (a) Complex impedance at various temperature and (b) activation energy for x=0.4 ceramic.

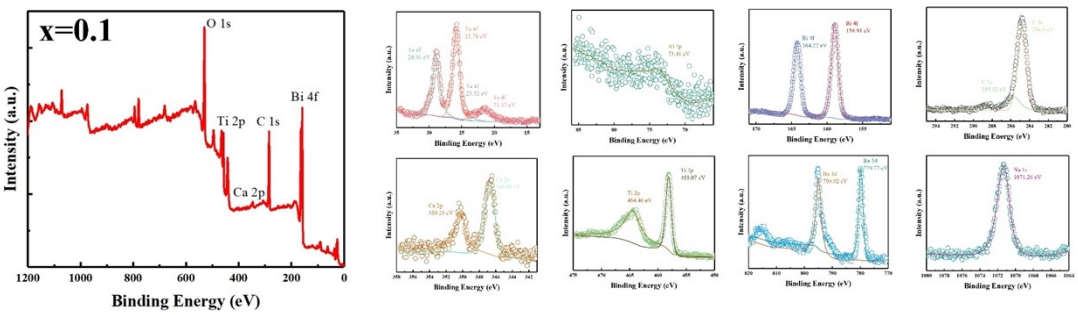

Fig. S11. XPS spectra for x=0.1 sample.

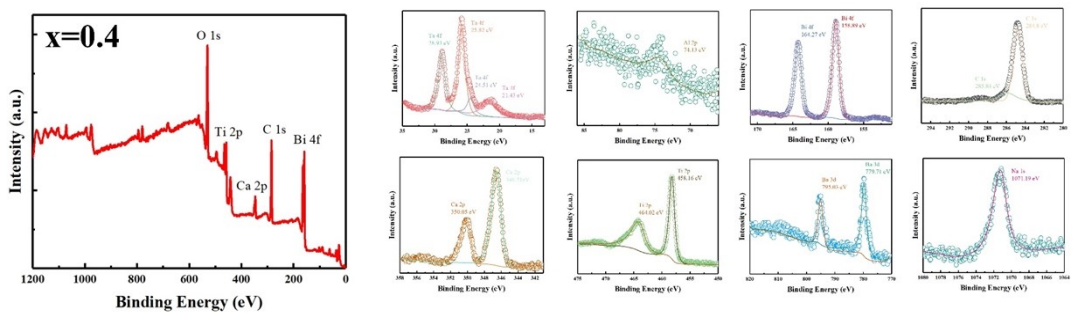

Fig. S12. XPS spectra for x=0.4 sample.

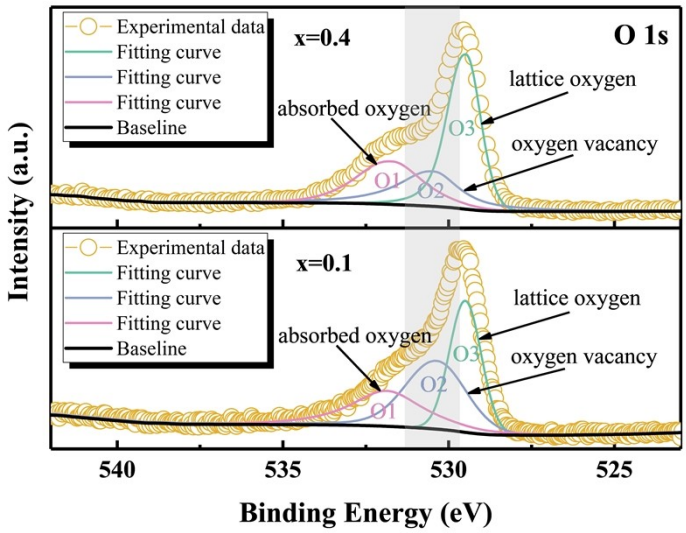

Fig. S13. XPS spectra of O 1s for BNT-BAT-0.4CT and BNT-BAT-0.1CT sample.

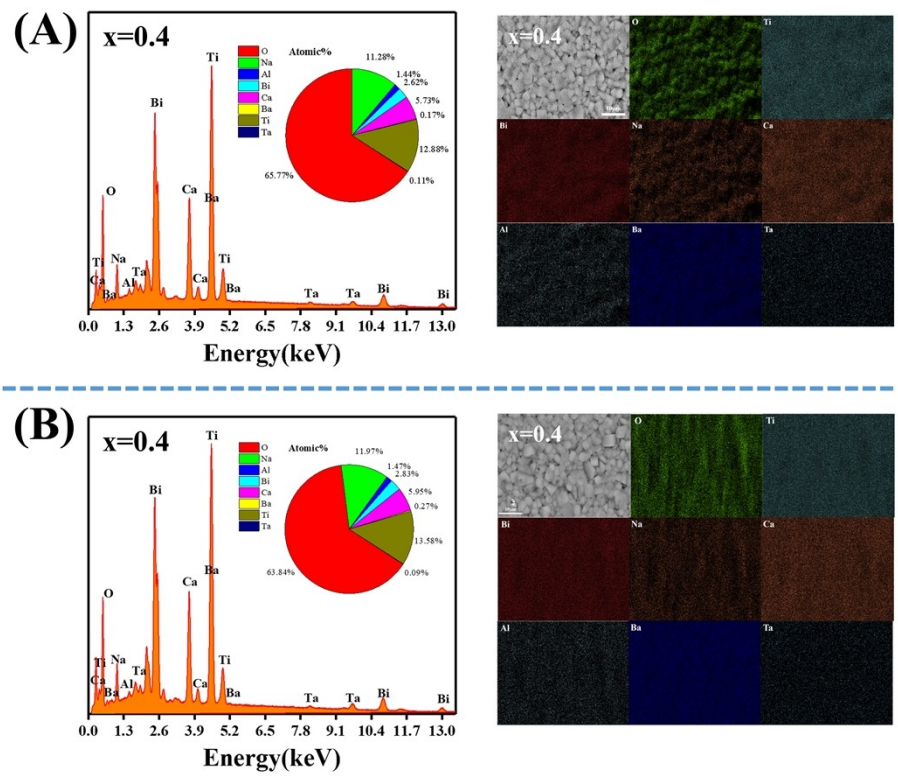

Fig. S14. Atomic percentage and EDS element mapping of the as-sintered surface (A) and the polished and thermally etched cross-sections (B) for BNT-BAT-0.4CT ceramics.

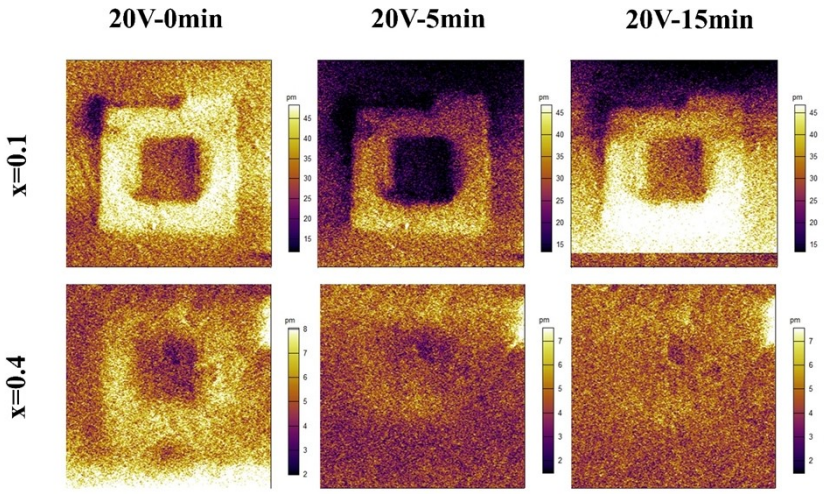

Fig. S15. Out-of-plane PFM amplitude images under different relaxation times after applying 20V voltage for the indicated ceramics.

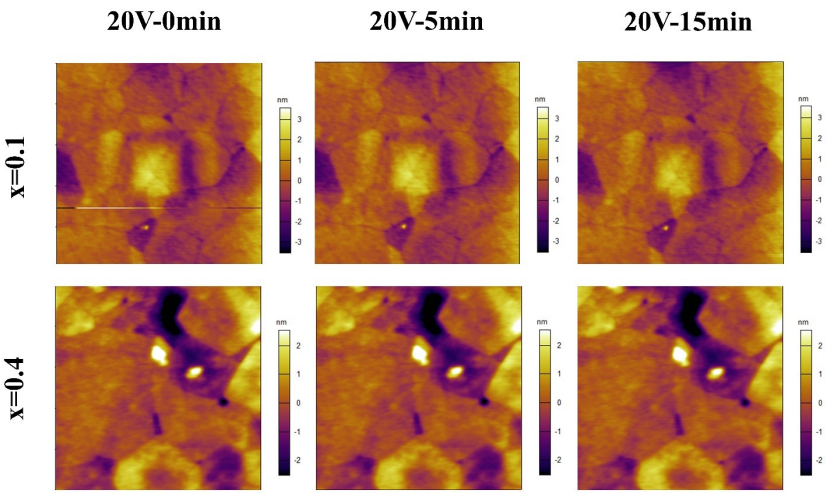

Fig. S16. Out-of-plane PFM morphology images under different relaxation times after applying 20V voltage for the indicated ceramics.

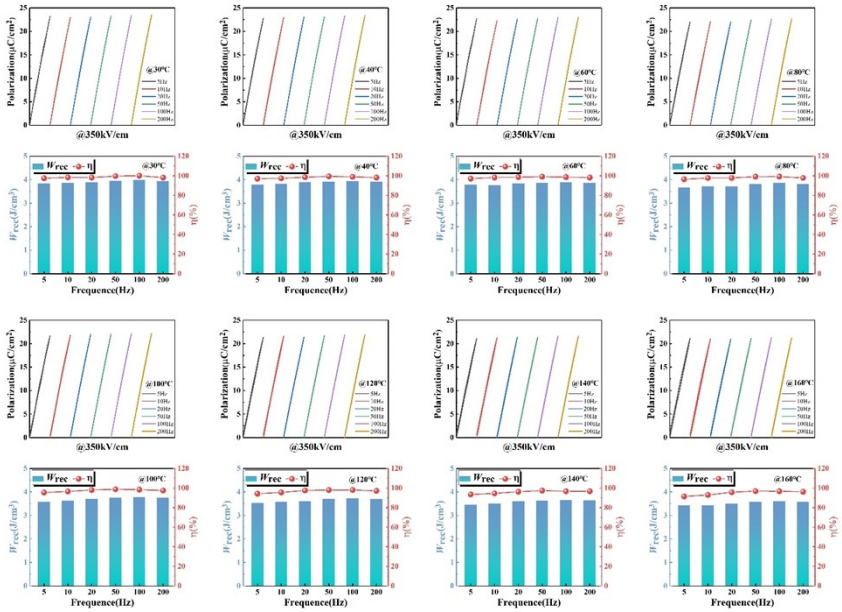

Fig. S17. Unipolar *P-E* loops and the change of W_{rec} and η as functions of temperature and frequency for BNT-BAT-0.4CT ceramic.

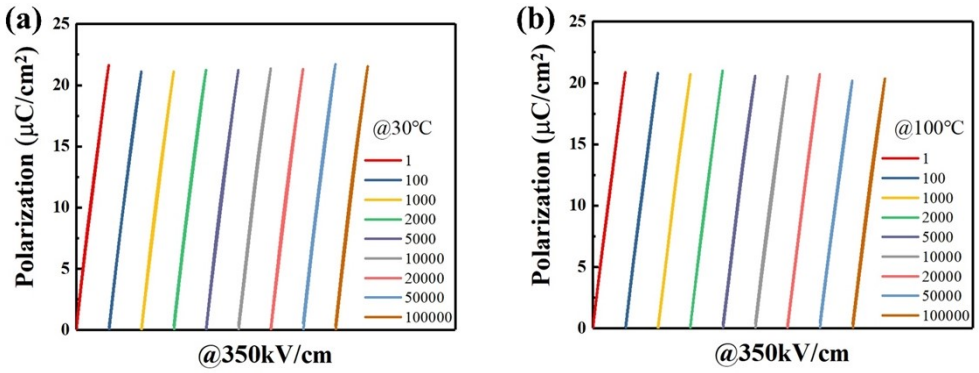

Fig. S18. Cycle number-dependent unipolar *P-E* loops measured at 30℃ and 100℃ for BNT-BAT-0.4CT ceramics.

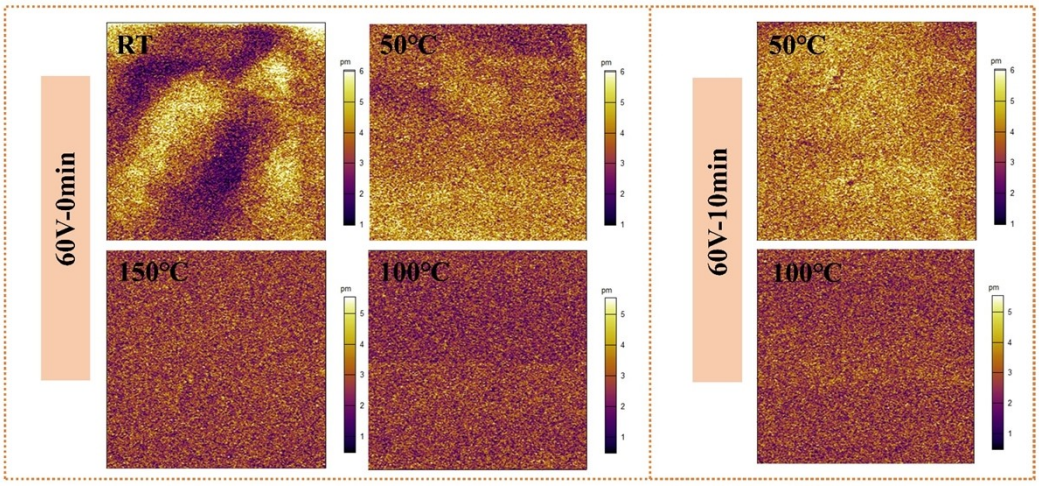

Fig. S19. Out-of-plane PFM amplitude evolution with different temperatures for the x=0.4 sample.

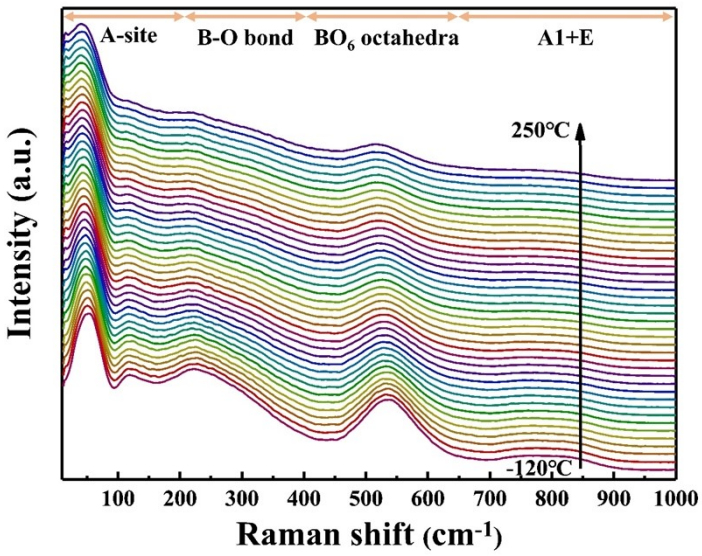

Fig. S20. Raman spectra of the BNT-BAT-0.4CT ceramic measured from -120℃ to 250℃.

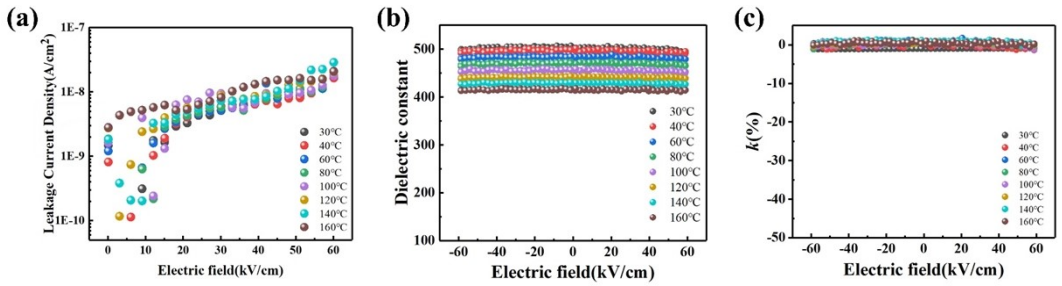

Fig. S21. Temperature-dependent (a) leakage current density, (b) dielectric constant, and (c) dielectric tenability for x=0.4 ceramic measured under 60 kV/cm.

References

1. Z. Cai, X. Wang, W. Hong, B. Luo, Q. Zhao and L. Li, *J. Am. Ceram. Soc.*, 2018, **101**, 5487-5496.
2. Z. Cai, X. Wang, L. Li and W. Hong, *Extreme Mech. Lett.*, 2019, **28**, 87-95.
3. Z. Cai, X. Wang, B. Luo, W. Hong, L. Wu and L. Li, *Compos Sci Technol*, 2017, **145**, 105-113.
4. K. C. Pitike and W. Hong, *J. Appl. Phys.*, 2014, **115**, 044101.
5. P. Zhao, Z. Cai, L. Chen, L. Wu, Y. Huan, L. Guo, L. Li, H. Wang and X. Wang, *Energy Environ. Sci.*, 2020, **13**, 4882-4890.
6. H. Ye, F. Yang, Z. Pan, D. Hu, X. Lv, H. Chen, F. Wang, J. Wang, P. Li, J. Chen, J. Liu and J. Zhai, *Acta Mater.*, 2021, **203**, 116484.
7. H. Pan, J. Ma, J. Ma, Q. Zhang, X. Liu, B. Guan, L. Gu, X. Zhang, Y.-J. Zhang, L. Li, Y. Shen, Y.-H. Lin and C.-W. Nan, *Nat. Commun.*, 2018, **9**, 1813.
8. Z. Hu, B. Ma, R. E. Koritala and U. Balachandran, *Appl. Phys. Lett.*, 2014, **104**, 263902.
9. I. Fujii, S. Trolier-McKinstry and C. Nies, *J. Am. Ceram. Soc.*, 2011, **94**, 194-199.
10. L. Wu, X. Wang, Z. Shen and L. Li, *J. Am. Ceram. Soc.*, 2017, **100**, 265-275.